

Self-Polarized BaTiO₃ for Greatly Enhanced Performance of ZnO UV Photodetector by Regulating the Distribution of Electron Concentration

Yong Zhang, Xiaoyue Zhao, Jiabin Chen, Siyuan Li, Wei Yang, and Xiaosheng Fang*

ZnO film ultraviolet photodetectors (UV PDs) have always suffered from slow speed and low photosensitivity that restrict their broader applications. To break through those barriers, high-performance ZnO UV PD based on self-polarized BaTiO₃ (BTO) is first introduced through a facile one-step spin-coating method. Compared with pure ZnO film UV PD with low on/off ratio (65) and slow speed (4.1/7.5 s) at 3 V bias under 350 nm UV light, the BTO-ZnO bilayer film device exhibits an ultrahigh on/off ratio (14 300) and ultrafast response speed (0.11/5.80 ms), which is much faster than that of the most reported ZnO film-based UV PDs. The numerical simulation demonstrates that the spatial distribution of electron concentration of ZnO film is regulated by the self-polarization of BTO film, resulting in low dark current and fast response time of the BTO-ZnO PD. This work provides a new approach to fabricate high-performance PDs based on self-polarized ferroelectric materials.

1. Introduction

Photodetectors (PDs), which detect irradiation directly by converting light into electrical signals, have attracted intensive attention in various fields, such as environmental monitoring, spectral analysis, image sensing, and communications.^[1–6] Zinc oxide (ZnO), a wide-bandgap transparent semiconductor, is one of the most popular materials in ultraviolet PDs (UV PDs) due to its strong exciton binding energy, high carrier mobility, low resistivity, and excellent photoconductivity properties.^[7–10] ZnO film devices demonstrate great potential in UV PDs field because of their structural simplicity, environmental friendliness, and large-scale and low-cost preparation. However, the practical applications of ZnO film UV PDs have been seriously hindered from their low on/off ratio (≈ 10) or long decay time (≈ 20 s) due to the influence of adsorption and desorption of surface oxygen molecules.^[11,12] A variety of methods have been reported


for improving the performance of ZnO devices including surface plasma modification, internal doping, heterojunction, and surface functionalization.^[13–17] Ouyang et al. integrated ZnO film UV PDs with CdMoO₄ microplates. Their strategy increased the on/off ratio to 34, and reduced the rise time and the decay time to 16/18 s, respectively.^[16] Jin et al. developed self-assembly of graphdiyne nanoparticles onto the surface of ZnO particles, and the ZnO-based UV device exhibited high on/off ratio and fast rise/decay time of 6.1/2.1 s, respectively.^[17] Nevertheless, these results are still not so satisfying for a wide range of practical applications. To develop ZnO UV PD with high on/off ratio and fast response speed is still a great challenge. Therefore, there is a significant and urgent

need to explore new approaches for high-performance ZnO UV PDs.

It is generally accepted that the response time and conductivity of the ZnO devices are greatly influenced by the depletion layer formed.^[18,19] Therefore, it is accessible to regulate the depletion layer by built-in electric fields of ferroelectric material.^[20] For instance, Wang et al. reported the feasibility of ferroelectric material in regulating the photoelectric properties. They employed a 300 nm P(VDF-TrFE) ferroelectric polymer to adjust the channel current of MoS₂ device.^[21] Zheng et al. presented a single CdS nanowire UV PD with enhanced on/off ratio (up to 10⁶) due to the polarization of ferroelectric polymer P(VDF-TrFE) by high electrostatic field.^[22] The intrinsic carriers in the CdS nanowire were depleted, reducing the dark current and enhancing the sensitivity of the device. Therefore, it is a reasonable approach to apply the ferroelectric material to enhance the performance of ZnO PDs. However, the ferroelectric polymer needs to be polarized by ultrahigh extra voltage, while complicated electrode preparation and polarization process hinder the utilization of polarized ferroelectric materials.

Barium titanate (BaTiO₃, BTO), a well-known ferroelectric material having high dielectric constant, low dielectric loss, and promising ferroelectric properties, has been exploited in many applications such as gas sensing, waveguide modulators, pressure transducers, capacitors, and memory devices.^[23–25] In addition, BTO film can be prepared by a simple sol-gel spin-coating method, which is compatible with the preparation of ZnO film.

Dr. Y. Zhang, X. Y. Zhao, J. X. Chen, S. Y. Li, W. Yang, Prof. X. S. Fang
Department of Materials Science
Fudan University
Shanghai 200433, P. R. China
E-mail: xshfang@fudan.edu.cn

 The ORCID identification number(s) for the author(s) of this article can be found under <https://doi.org/10.1002/adfm.201907650>.

DOI: 10.1002/adfm.201907650

Most importantly, BTO has excellent self-polarization characteristic, thereby a macroscopic polarization appears naturally in ferroelectrics without electrode and external electric field.^[26,27] There are several mechanisms that have been proposed to explain self-polarization phenomenon such as the gradients of charge deficiency near the surface and compressive epitaxial strain.^[28–30] For instance, Chen et al. observed upward ferroelectric self-polarization in BTO films on (001)-oriented SrTiO₃ and Nb-SrTiO₃ substrates. They concluded that the lattice mismatch between BTO films and SrTiO₃ substrate induced the inhomogeneous epitaxial strain that coupled with polarization leading to the upward self-polarization.^[31] This special property provides great convenience to design BTO film for the UV detectors. Therefore, BTO could be a promising ferroelectric material to improve the photoelectric performance of ZnO film device.

In this work, we successfully achieved the BTO-ZnO bilayer film by a simple one-step spin-coating and annealing process. The BTO-ZnO bilayer film UV PD demonstrates an ultrahigh on/off ratio and ultrafast response speed, while pure ZnO film device show low on/off ratio and slow speed at 3 V at 350 nm light illumination. The self-polarized BTO film was characterized by piezoresponse force microscope, and the self-polarized electric field is measured by source-meter analyzer. Under the electric field produced by self-polarized BTO film, the spatial distribution of carrier concentration of ZnO film was simulated by the finite element method (FEM). These results potentially make self-polarization ferroelectric films promising candidates for high-performance PDs.

2. Results and Discussions

In order to investigate the feasibility of enhancing the photoelectric performance of ZnO PD, the ferroelectric BTO film was employed to integrate with ZnO film through a facile one-step spin-coating method. The schematic diagrams for preparation of the pure ZnO PD and the composite BTO-ZnO bilayer film PD are depicted in **Figure 1a,b**, respectively. The ZnO and BTO solutions were prepared and sequentially spin-coated on clean quartz substrates followed by annealing at 700 °C for 2 h. Note that the ZnO solution was spin-coated immediately after the BTO film was heated at 300 °C for 10 min to ensure in situ growth of the self-polarization. Two small indium pieces were pressed onto the BTO-ZnO film as the electrodes to build the device. Indium is chosen as the electrodes to guarantee ohmic contact with ZnO film. The photoelectric properties of the as-prepared devices were investigated at room temperature by using a two-probe method. **Figure 1c–f** display the scanning electron microscopy (SEM) images of the BTO film and BTO-ZnO composite film with different magnifications. As shown in **Figure 1c,d**, the BTO film deposited on the quartz substrate consists of densely packed nanoparticles. **Figure 1e,f** demonstrates that the ZnO nanoparticles with diameters of 50–100 nm are aligned closely to form a dense and homogeneous film on the surface of BTO film. Both the ZnO and BTO films showed good uniformity, excellent compactness, and high density. In addition, no obvious macroscopic cracks are observed on the surface of the films. To survey the interface of the as-prepared

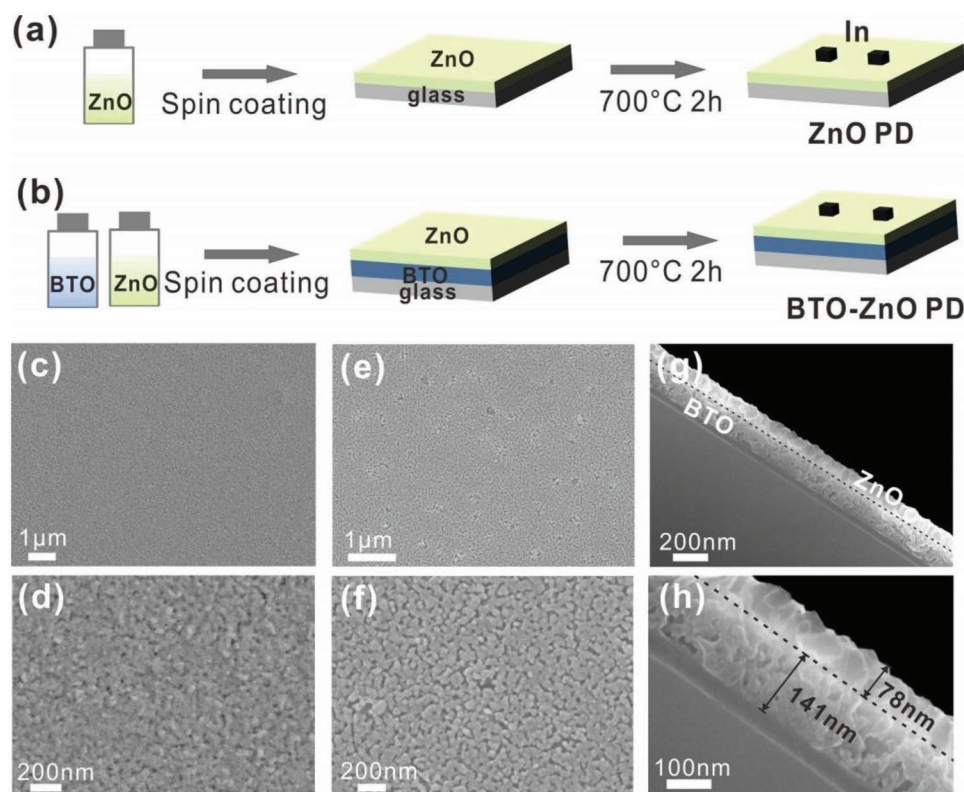


Figure 1. Schematic diagram showing the preparation for a) ZnO PD and b) BTO-ZnO PD. SEM images of c,d) the BTO film and e,f) the ZnO film with different magnification. g, h) Cross-sectional images of the BTO-ZnO film.

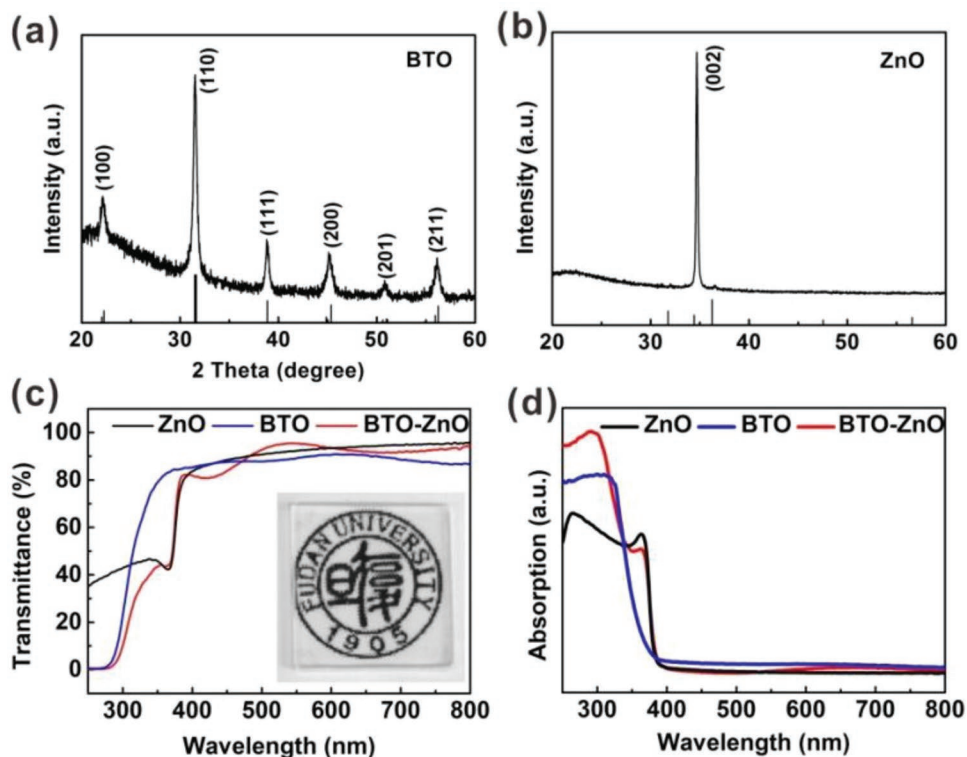


Figure 2. XRD patterns of a) BTO film and b) ZnO film. c) Transmittance spectra of the ZnO film, BTO film, and BTO-ZnO film. d) UV-vis absorption spectra of the ZnO film, BTO film, and BTO-ZnO film.

BTO-ZnO film, cross-sectional identification was carried out and shown in Figure 1g,h. It is clearly seen that there are two kinds of nanoparticles with different diameters, indicating an obvious smooth interface between BTO layer and ZnO layer. With a closer observation of the interface in Figure 1h, the different nanoparticles were staggered together forming a well-interacted interface after annealing, which is helpful to transfer carriers at the interface. The thicknesses of the BTO layer and ZnO layer are calculated to be 141 and 78 nm, respectively. These results indicate that a well-defined BTO-ZnO bilayer film with good compactness and smoothness was successfully prepared via a simple one-step solution progress. The as-prepared BTO film provides a promising platform to integrate with other semiconductor materials for various devices.

The crystalline structure of the BTO and ZnO films is characterized by X-ray diffraction (XRD) patterns. As seen in Figure 2a, the diffraction peaks located at 22.3° , 31.6° , 38.9° , 45.4° , 51.0° , and 56.3° correspond to the (100), (110), (111), (200), (201), and (211) crystal planes of BTO (JCPDS No. 05-0626), respectively. All the peak positions and their relative intensities are in good agreement with the tetragonal phase lattice constants of $a = b = 3.994 \text{ \AA}$, $c = 4.038 \text{ \AA}$. The linewidth of all the peaks are large, which indicates that BTO nanoparticles are of very small diameter. From Figure 2b, the strong peak located at 34.4° is assigned to the (002) plane of ZnO (JCPDS No. 65-3411), with the lattice parameters of $a = b = 3.249 \text{ \AA}$, $c = 5.207 \text{ \AA}$. This sharp and strong peak indicates the high crystallinity ZnO film and the film is exposed with the (002) plane. In order to investigate the composition and electronic states of the as-prepared

samples, X-ray photoelectron spectroscopy (XPS) measurements were carried out by using element C for calibration, as displayed in Figure S1, Supporting Information. Figure S1a, Supporting Information, depicts the XPS full spectra of the ZnO and BTO films and provides the detailed information of the Zn 2p_{3/2}, O 1s, Ba 3d₅, Ti 3d₅, O 1s peaks, indicating the chemical composition of ZnO and BTO films. The spin-orbit splitting peaks corresponding to Zn 2p_{3/2} and Zn 2p_{1/2} with 1021 and 1045 eV, respectively, demonstrate the existence of Zn²⁺ in sample (Figure S1b, Supporting Information). The O 1s spectrum of ZnO film is fitted with two Gaussian peaks, which has two binding energy components as reported in previous literature (Figure S1c, Supporting Information).^[32] Peak I, positioned at the lower binding energy of 529.58 eV, is attributed to O²⁻ ions in the Zn-O bonding of the wurtzite structure of ZnO.^[32] Peak II, the higher binding energy at 531.75 eV, is assigned to the Zn-OH bonding.^[33] The XPS spectra of Ba 3d₅ and Ti 3d₅ displayed in Figure S1d,e, Supporting Information, indicate the normal state of Ba²⁺ and Ti⁴⁺ in the BTO film. Figure S1f, Supporting Information, shows the O 1s spectra of BTO with two components: peak I of 530.47 eV is attributed to oxygen in the perovskite environment, while peak II of 532.69 eV is ascribed to hydroxyl groups chemically bonded to surface.^[34–36]

The optical transmittance spectra from 800 to 250 nm of the BTO, ZnO, and BTO-ZnO films are measured and displayed in Figure 2c. The BTO film and ZnO film both possess a high transmittance of $\approx 90\%$ within the visible light region. The transmittance of BTO-ZnO bilayer also exhibits a high value of

≈90%. It indicates that the BTO-ZnO film is transparent, which is also confirmed from the digital images inserted in Figure 2c. The UV-vis absorption spectra of the ZnO, BTO, and BTO-ZnO films were investigated on quartz glass to study their optical properties, as presented in Figure 2d. It is worth noting that the BTO-ZnO composite film exhibits two peaks, corresponding to that of the BTO film and ZnO film. The absorbance of ZnO dominates from 380 to 340 nm, while the absorbance of BTO-ZnO bilayer film increases from 340 to 300 nm that is attributed to the absorbance caused by the BTO film. These results revealed that the as-prepared BTO-ZnO film can act as a promising candidate for transparent UV detectors due to its excellent selectivity in UV absorption and high transmittance in the visible region. As shown in Figure S2a,b, Supporting Information, the bandgaps of as-prepared ZnO and BTO particles films are estimated to be 3.28 and 3.52 eV by the Tauc plots according to the UV-vis absorbance spectroscopy, respectively.^[37,38]

In order to enhance the performance of ZnO film PD, BTO film was integrated to form BTO-ZnO bilayer film. The comparison of photoelectric performance between pure ZnO and composite BTO-ZnO film devices was investigated as displayed in Figure 3. Figure 3a exhibits the typical current-voltage (I - V) curves of the ZnO and the BTO-ZnO PDs in a logarithmic plot in dark and under 350 nm light illumination. The I - V curves of the ZnO film metal-semiconductor-metal structure with In electrodes show symmetrical characteristic under dark condition, indicating ohmic contacts between ZnO film and In electrodes. For pure ZnO film PD, the current increases remarkably from 30 pA in dark to 6 nA under 350 nm light illumination at 3 V bias voltage. The initial on/off ratio of this device reaches 200, indicating that ZnO film is an excellent candidate to develop high-performance PDs. For pure BTO film PD, no obvious photoresponse is detected in dark and under 350 nm light illumination (Figure S3, Supporting Information). Surprisingly, when the BTO film was integrated with ZnO

film, the current of BTO-ZnO film under illumination greatly increases to 20 nA, and the dark current significantly reduces to 3 pA. The dark current of the BTO-ZnO PD is much lower than that of ZnO PD, which may be caused by the depletion layer formed by the self-polarization of BTO film. Meanwhile, the photocurrent of BTO-ZnO PD is higher than that of the ZnO PD that is attributed to the decrease of the recombination of carriers by the self-polarized electric field. The reproducibility of photoresponse is very important for high-performance PDs. Figure 3b exhibits the photocurrent response curves of ZnO PD and BTO-ZnO PD irradiated with 350 nm light at 3 V bias. The current-time (I - t) characteristics of both devices show good reproducibility without noticeable photocurrent decay. For BTO-ZnO PD, the photocurrent rapidly increases to a steady state of 20 nA and then quickly decreases to 1 pA, with UV light on-off switching, respectively. This indicates a rapid separation of electron-hole pairs caused by BTO film near the interface. By contrast, the current of the ZnO PD rises slowly to 6 nA and decays extremely slowly to 0.1 nA in the initial state with periodical on/off UV light illumination. The BTO-ZnO PD has high performance with fast and stable photoresponse. This indicates that the BTO ferroelectric layer has a positive effect on the photoelectric performance of ZnO device.

The response time and photosensitivity are key parameters to evaluate the performance of UV PDs. The photosensitivity can be defined as the ratio of photocurrent to dark current (I_{ph}/I_d). Figure 3c shows a single period of the I - t curves on a semi-logarithmic plot upon 350 nm UV irradiation (0.91 mW cm²) to calculate the on/off ratio of the ZnO and BTO-ZnO PDs. For pure ZnO PD, the current decays slowly to 0.1 nA in 60 s, leading to a low on/off ratio of 65. For the BTO-ZnO PD, the photocurrent rapidly decreases to 1 pA under the same condition. Due to the dramatic decrease in dark current and the pronounced increase in the photocurrent, the on/off ratio of the BTO-ZnO PD incredibly increases to 14 300, which is 220 times

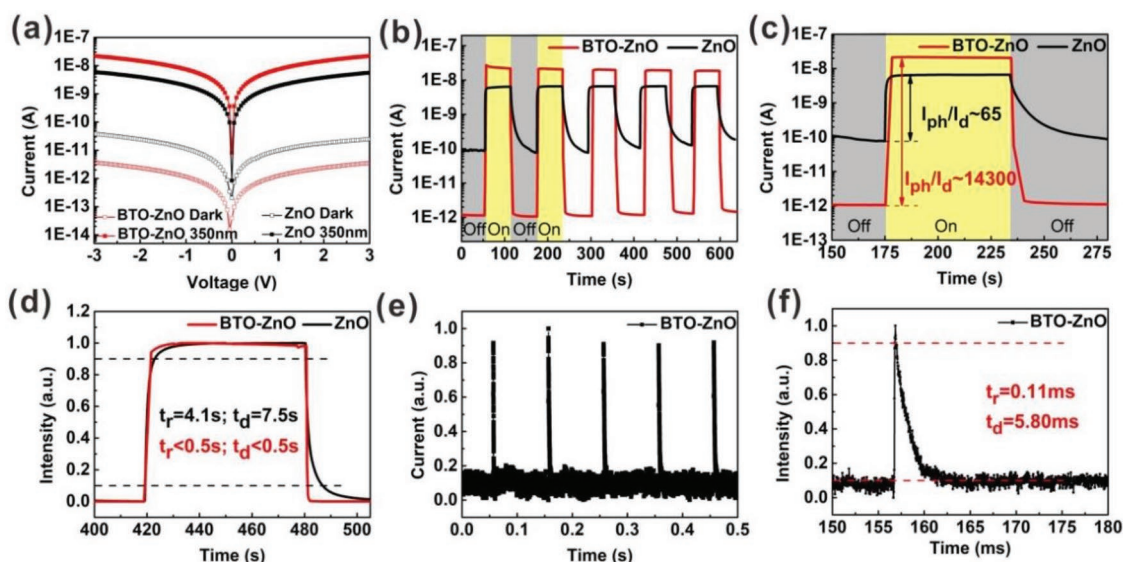


Figure 3. Comparison of photoelectric performance between ZnO PD and BTO-ZnO PD. a) I - V characteristics and b) I - t characteristics under dark and 350 nm light. c) Single period of the I - t curve and d) the normalized I - t curves. e) Photoresponse of BTO-ZnO PD under 3 Hz 355 nm laser pulse and f) the normalized single pulse response.

than that of ZnO PD. In order to compare the response time of the ZnO and BTO-ZnO PDs, the time-dependent current curves are normalized and shown in Figure 3d. The rise time (the peak photocurrent rises from 10% to 90%) and the decay time (the peak photocurrent decays from 90% to 10%) are calculated to be 4.1 and 7.5 s for ZnO PD, respectively. It is obvious that the BTO-ZnO PD has fast response speed, and the rise and decay times are less than 0.5 s. Regarding the limitation of the sampling speed of the semiconductor characterization system (Keithley 4200-SCS), a quick response measure system is applied to evaluate the precise response speed of the BTO-ZnO PD with 350-nm pulsed laser. In order to get the rise and decay time of the device in depth, five cycles of the pulse response of the BTO-ZnO PD are recorded and shown in Figure 3e. Results shown testify the fast speed and repeatability of the device. Figure 3f shows the normalized curve of a single period of the pulse response as a function of time. The rise time and the decay time of BTO-ZnO PD is calculated as 0.11 and 5.80 ms, respectively, one thousandth of the rise/decay time of the ZnO PD. Compared with single ZnO film UV detector of low on/off ratio (65) and slow speed (4.1/7.5 s), the BTO-ZnO bilayer film device exhibits a dramatically improved on/off ratio (14 300) and ultrafast response speed (0.11/5.80 ms), which is much faster than that of the most reported ZnO film-based PDs in literature (Table S1, Supporting Information). These results reveal that the self-polarization of BTO film not only acts as a depletion layer to reduce the dark current, but also can regulate the behaviors of carriers to accelerate response speed.

Figure 4a displays the I - V characteristics of the BTO-ZnO PD under 350 nm UV light illumination with different power densities. With increasing the power density from 0.232 to

1.028 mW cm^{-2} , the photoresponse of the device increases with photocurrent values of 5.158 nA at 0.232 mW cm^{-2} , 10.36 nA at 0.528 mW cm^{-2} , 15.45 nA at 0.739 mW cm^{-2} , 19.23 nA at 0.961 mW cm^{-2} , 20.30 nA at 1.028 mW cm^{-2} at 3 V under 350 nm light. This result corresponds well to the fact that the photo-generation efficiency of charge carriers is proportional to the absorbed photon flux. The nonlinear relationship for the variation of photocurrent against light intensity can be fitted by the power law

$$I_{\text{ph}} = AP^\theta \quad (1)$$

where, I_{ph} refers to photocurrent, P refers to irradiation intensity, while A is a constant with a certain wavelength and the response of the photocurrent to irradiation intensity is determined by the exponent ($0.5 < \theta < 1$). From the fitted curve in Figure 4b, the value of the exponent is calculated to be 0.95 at 3 V under 350 nm light. This fractional power dependence is related to the complex behaviors of electron-hole generation and recombination in the BTO-ZnO PD. The spectral responsivity (R_λ) is a critical parameter defined as photocurrent per unit of incident power, which presents the efficiency of a detector responding to optical signals. It can be calculated as

$$R_\lambda = (I_{\text{ph}} - I_{\text{d}})/(PS) \quad (2)$$

where I_{ph} is the photocurrent, I_{d} is the dark current, λ is the irradiation wavelength, P and S are the light power density and the effective irradiated area, respectively. For both the ZnO PD and BTO-ZnO PD, the diameter of electrodes and the channel length are about 0.2 and 0.1 cm, respectively. So

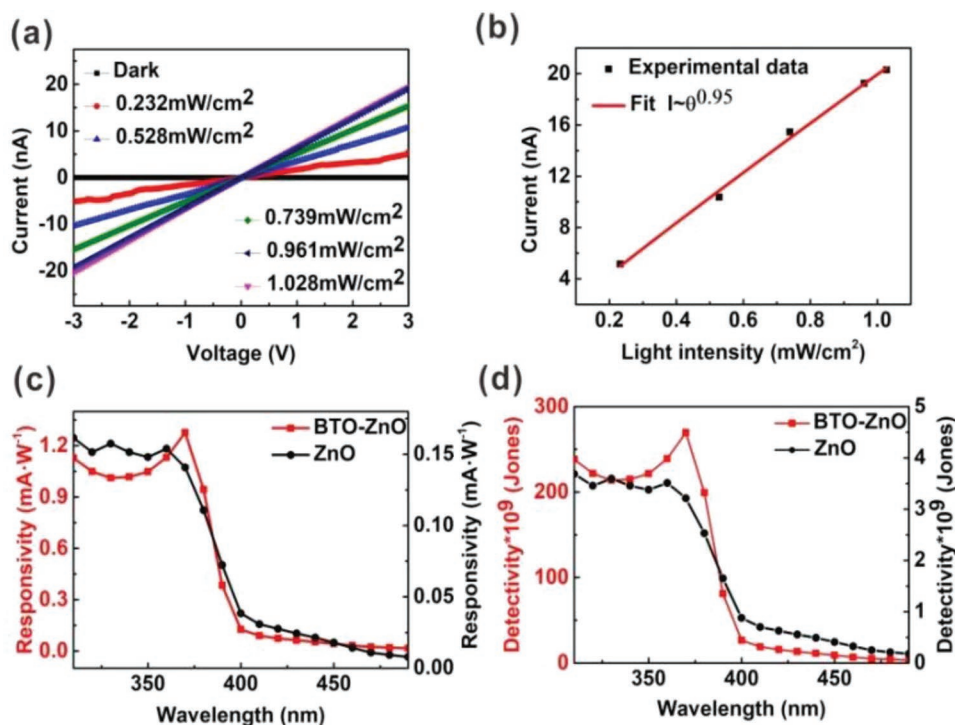


Figure 4. a) I - V characteristics of BTO-ZnO PD with various intensities. b) Photocurrent of the BTO-ZnO PD versus light intensity and corresponding fitted curve using the power law. c) Spectral response and d) detectivity of ZnO PD and BTO-ZnO PD, respectively.

the effective irradiated area is measured to be 0.02 cm². The spectral responsivities of the ZnO and BTO-ZnO PDs at 3 V bias from 500 to 300 nm are shown in Figure 4c. For ZnO PD, the responsivity is 0.14 mA W⁻¹ at the wavelength of 370 nm, and its spectral responsivity is significantly enhanced in the ultraviolet range. For the BTO-ZnO PD, the maximum responsivity of 1.28 mA W⁻¹ is achieved at 370 nm, which is about 10 times than that of ZnO PD. This result is mainly caused by the increase in photocurrent. Additionally, the BTO-ZnO PD shows low responsivities to light above 400 nm, indicating its excellent UV light selective response characteristics. The detectivity (D^*) reflects the ability of a device to detect weak light signals from the noise environment. By assuming the shot noise from the dark current is the major contributor, the detectivity (D^*) can be calculated as

$$D^* = R_\lambda / (2eI_d/S)^{1/2} \quad (3)$$

The detectivities of ZnO and BTO-ZnO PDs from 500 to 300 nm are shown in Figure 4d. As the result of the suppressed dark current and enhanced responsivity, the detectivity of the BTO-ZnO PD reaches to 2.70×10^{11} Jones at the wavelength of 370 nm that is much higher than that of the ZnO PD (3.21×10^9 Jones). Such an enhancement in detectivity might be attributed to the built-in electric field formed by in situ self-polarization of the BTO layer. The inner electric field can deplete the carriers at the interface, causing the great reduction of the dark current.

Piezoresponse force microscopy (PFM) is conducted to confirm the self-polarization phenomenon of BTO film. The self-polarization orientation of the BTO film is shown in Figure 5. For the out-of-plane phase image in Figure 5a, the domain with the negative phase accounts for the majority, showing that the out-of-domain is a single domain structure. The most self-polarization orientation is focused on -90° phase as clearly seen in Figure 5b. The size of the domain is about 100 nm (Figure 5c). The morphology of the in-plane domain indicates that the in-plane domain does not have a single domain structure. The phase image in Figure 5d confirms this result, and the in-plane domain shows two orientations concentrated at -90° and 90° phases, respectively. As a result, the amounts of the domain with negative phase offset those with positive phase. This self-polarization of BTO film is further confirmed by polarizing with extra high voltage. The hysteresis curve is measured on the BTO film and shown in Figure 5e,f. The result demonstrates that the built-in electric field is approximately 2.3 V cm⁻¹. Figure 5g displays the proposed built-in electric field formed by ferroelectric

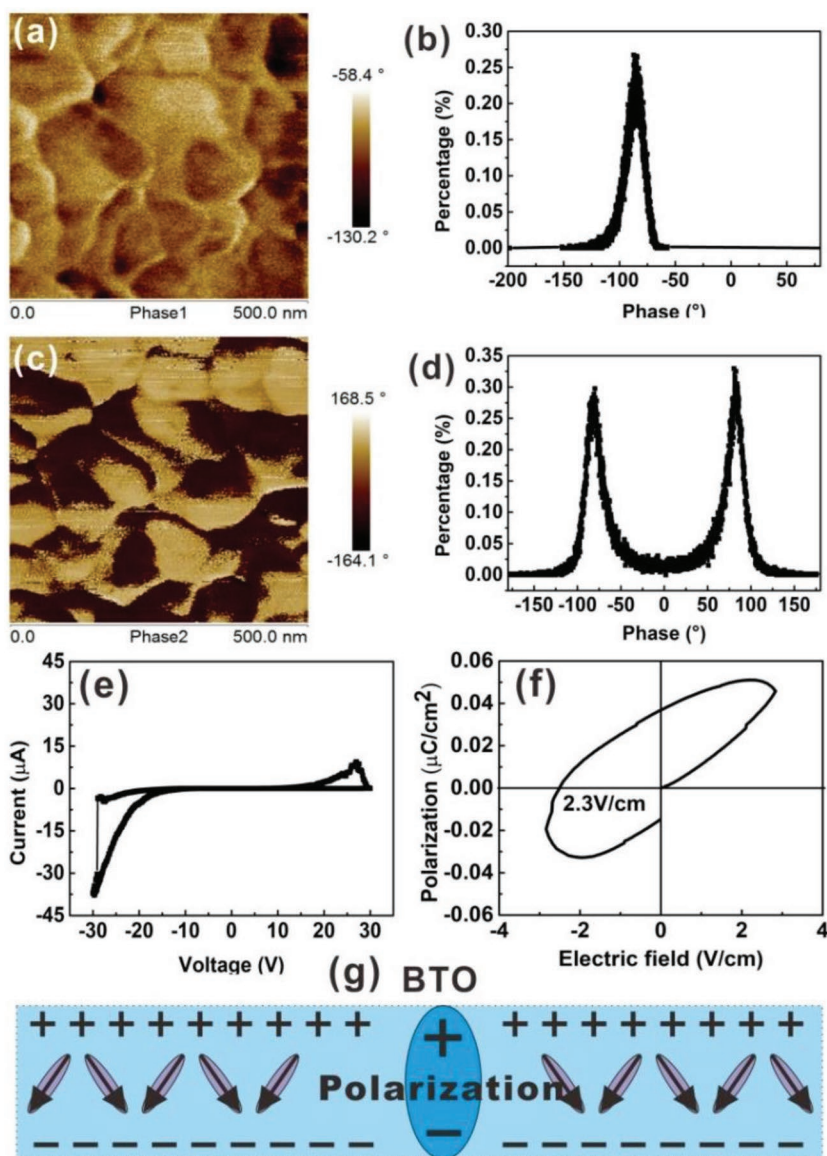


Figure 5. PFM images of the BTO film: a,b) out-of-plane phase image; c,d) in-plane phase image. e) The C–V curve of BTO film. f) The hysteresis curve of BTO film. g) Schematic diagram of the built-in field formed by the self-polarization orientation of BTO film.

self-polarization in the BTO film. A large number of polarization domains face right and left, while the number of domains faces down. As a result, an electric field with a downward direction is generally generated. Furthermore, in order to investigate the effect of the built-in electric field, the controlled experiment was carried out. The BTO-ZnO* film was prepared by a two-step method. As depicted in Figure S4, Supporting Information, the I – V curve of the BTO-ZnO* PD demonstrates that the device has good photoresponse with significant differences between the light and dark currents (Figure S4a, Supporting Information), and the I – t curve shows excellent stability and repeatability of the BTO-ZnO* device (Figure S4b, Supporting Information). Nevertheless, the BTO-ZnO* PD exhibit low on/off ratio of 60 close to that of the ZnO film (≈ 65) (Figure S4c, Supporting Information). The rise time and decay time of the

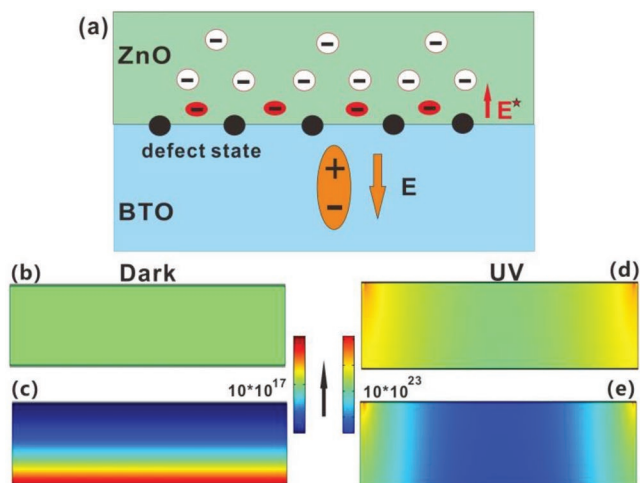


Figure 6. a) Simplified schematic diagrams of the electric field in the BTO-ZnO bilayer film. Spatial distribution of electrons concentration of b,d) pure ZnO and c,e) composite ZnO (BTO-ZnO) by FEM simulation in dark and under UV light illumination, respectively.

device is 2.8 and 3.37 s, respectively (Figure S4d, Supporting Information), little faster than that of bare ZnO film (4.1 and 7.5 s). This result revealed that the self-polarization electric field is shielded during the two-step progress. The BTO-ZnO film was only prepared by one-step progress, and the in situ self-polarization can exert great influence on the ZnO film.

To gain more insight into the mechanism of the BTO-ZnO film PD, the simplified schematic diagram of the electric field (E) formed by self-polarization is illustrated in **Figure 6a**. Particularly, the ZnO film is subjected to a downward electric field because of the majority of the domains with the polarization vector of BTO film face downward. In order to satisfy the electrostatic equilibrium, a number of electrons of ZnO film gather at the interface to generate an upward built-in electric field (E^*). This built-in electric field (E^*) can regulate the spatial distribution of electron concentration of ZnO, and then improve the photoelectric performance of the BTO-ZnO device. The spatial distributions of the electron concentrations of pure ZnO and BTO-ZnO PDs were simulated by the FEM based on COMSOL Multiphysics software. As shown in Figure 6b–e, the spatial distributions of the electron concentrations of ZnO were simulated in dark and under UV light illumination separately.^[39] For pure ZnO device, the slow adsorption and desorption process of oxygen molecules on the upper surface of ZnO film leads to low on/off ratio and the long response time. For BTO-ZnO device, the built-in electric field (E^*) forms the depletion layer, leading to the extreme low dark current (1pA) in dark. Under UV light illumination, the decreasing electron concentration of ZnO reduces the recombination probability of carriers, which can improve the photocurrent of BTO-ZnO PD. The built-in electric field is very beneficial to accelerate the recombination of the electrons and holes on the lower surface of ZnO film, leading to fast response time of the BTO-ZnO device. In addition, due to the mismatch of lattice parameters between BTO and ZnO, the strain induced at the interface will produce a large number of defect states. The photogenerated carriers will be transferred and recombined rapidly by the defect states.^[40–42]

Therefore, the response time of the BTO-ZnO device is greatly improved. In brief, the in situ self-polarization electric field produced by the BTO film contributed for the great enhancement in the photoelectric properties of ZnO PD, thereby exhibiting the high on/off ratio and fast response speed.

3. Conclusion

In summary, the high-performance BTO-ZnO UV PD was fabricated by a low-cost and simple solution-processed method. The single ZnO UV PD displays low on/off ratio (65) and slow speed (4.1/7.5 s) at 3 V at 350 nm, but the BTO-ZnO bilayer film device demonstrates an ultrahigh on/off ratio (14 300) and ultrafast response speed (0.11/5.80 ms), exceeding those of most current ZnO film-based PDs. A downward self-polarization of BTO film was observed by PFM imaging, and the self-polarized electric field is measured to be about 2.3 V cm^{-1} . Because the spatial distribution of electron concentration of ZnO film was regulated by numerical simulation under the self-polarized electric field of BTO film, the BTO-ZnO PD demonstrates low dark current and fast response speed. The strategy of employing self-polarized ferroelectric materials provides a facile way to design and fabricate high-performance PDs for practical applications.

4. Experimental Section

Preparation of ZnO Film: All the chemicals were purchased from Aladdin and were used as received without further purification. Typically, 1.44 g of $\text{Zn}(\text{CH}_3\text{COO})_2 \cdot 2\text{H}_2\text{O}$ and 0.75 g of poly(vinyl alcohol) (PVA-1788, Mw = 44) were dissolved in 9 mL water and 1 mL ethanol. Later, 0.5 mL of acetic acid was added to the as-prepared solution and stirred for 60 min at room temperature to restrain the hydrolysis of zinc salt. Several quartz substrates were washed by acetone, ethanol, and deionized water. The solution was spin-coated on clean quartz substrates at a speed of 3000 rpm for 30 s. Finally, the samples were annealed in air at $700 \text{ }^\circ\text{C}$ for 2 h with a heating rate of $5 \text{ }^\circ\text{C min}^{-1}$.

One-Step Preparation of BTO-ZnO Film: First, 0.08 g PVP (Mw = 5500) was dissolved in 6.0 g isopropyl alcohol. Then 2.27 g acetic acid and 1.46 g titanium isopropoxide were added to form solution A. Meanwhile, 1.28 g barium acetate was dissolved into 1.8 g H_2O forming solution B. Solutions A and B were separately stirred for 60 min and the solution B was added dropwise into solution A, followed by stirring for another 60 min. Then the obtained BTO solution was spin-coated on clean quartz substrates at a speed of 5000 rpm for 60 s and immediately heated on hot plate ($300 \text{ }^\circ\text{C}$) for 10 min. Subsequently, the ZnO solution was spin-coated on the surface of BTO film at a speed of 3000 rpm for 30 s. Finally the samples were annealed in air at $700 \text{ }^\circ\text{C}$ for 2 h at a rate of $5 \text{ }^\circ\text{C min}^{-1}$.

Two-Step Preparation of BTO-ZnO* Film: To make a comparison, two-step method was introduced. The first step is to prepare the BTO film by sol-gel spin-coating method and annealing at $700 \text{ }^\circ\text{C}$ for 2 h. The second step is to obtain BTO-ZnO* film by spin-coating the ZnO solution on the surface of BTO film and annealing in air at $700 \text{ }^\circ\text{C}$ for 2 h again.

Analysis Instruments: XRD was tested to confirm the crystal structures of the samples by using a Bruker D8-A25 diffractometer with Cu $K\alpha$ radiation ($\lambda = 1.5405 \text{ \AA}$). Field-emission SEM (Zeiss Sigma) was used to examine the morphology of the samples. PFM imaging of all domains was measured by using an AFM in ScanAsyst-air mode (Bruker Icon) using a contact PtIr-coated silicon tip with a radius of 20 nm, a force constant of 2.8 N m^{-1} , and an alternating current frequency of 75 kHz and an amplitude of 10 V. The XPS spectra of the samples were

investigated by a Perkin Elmer PHI 5000C ESCA system equipped with a hemispherical electron energy analyzer, and the Mg-K α (1253.6 eV) anode was operated at 14 kV and 20 mA. All the binding energy for C1s peak at 284.6 eV was used as the reference for calibration. A UV-vis spectrophotometer (Hitachi U-3900H) with an integrating sphere attachment was used to measure the optical properties by optical absorption spectra. Ferroelectric property of the BTO film was measured via a precise source-meter analyzer (B2902A, Keysight).

Photoelectric Measurements: To construct PDs, two small pieces of indium metal with fixed areas were pressed onto the films as electrodes. The photoelectric properties of the as-prepared devices (the current-time transient response and the current-voltage characteristic) were evaluated with a program-controlled semiconductor characterization system (Keithley 4200, USA). The light intensity was detected by a NOVA II power meter (Ophir Photonics). For the precise measurement of the photoresponse, a YAG:Nd laser (pulse duration: 3–5 ns, 355 nm, Continuum Electro-Optics, Minilite II) with a 1 G Ω resistor and an oscilloscope (Tektronix MSO/DPO5000) was used. The carrier concentration spatial distribution of ZnO film was simulated by the FEM based on COMSOL Multiphysics software. All the measurements were performed at room temperature under ambient conditions.

Supporting Information

Supporting Information is available from the Wiley Online Library or from the author.

Acknowledgements

Y.Z. and X.Z. contributed equally to this work. The authors would like to thank Guoyang Cao for simulating the carrier concentration spatial distribution of ZnO film. This work was supported by the National Key Research and Development Program of China (Grant No. 2018YFA0703700), Fudan's Undergraduate Research Opportunities Program (FDUROP, Grant No. 18023), the National Natural Science Foundation of China (NSFC Grant Nos. 51872050, 11674061, and 11811530065), the Ministry of Education Joint Fund for Equipment Pre-Research (6141A02033241), and Science and Technology Commission of Shanghai Municipality (Grant Nos. 18520744600, 18520710800, and 17520742400). Part of the research was carried out in Fudan Nanofabrication Laboratory.

Conflict of Interest

The authors declare no conflict of interest.

Keywords

BaTiO₃ film, self-polarization, UV photodetector, ZnO film

Received: September 16, 2019

Revised: October 23, 2019

Published online: November 18, 2019

- [1] W. Yang, J. X. Chen, Y. Zhang, Y. J. Zhang, J. H. He, X. S. Fang, *Adv. Funct. Mater.* **2019**, *29*, 1808182.
- [2] C. H. Lin, B. Cheng, T. Y. Li, J. R. D. Retamal, T. C. Wei, H. C. Fu, X. S. Fang, J. H. He, *ACS Nano* **2019**, *13*, 1168.
- [3] A. M. AlAmri, S. F. Leung, M. Vaseem, A. Shamim, J. H. He, *IEEE Trans. Electron Devices* **2019**, *66*, 2657.

- [4] H. P. Wang, D. Periyangounder, A. C. Li, J. H. He, *IEEE Access* **2019**, *7*, 19395.
- [5] F. Wang, Z. X. Wang, L. Yin, R. Q. Cheng, J. J. Wang, Y. Wen, T. A. Shifa, F. M. Wang, Y. Zhang, X. Y. Zhan, J. He, *Chem. Soc. Rev.* **2018**, *47*, 6296.
- [6] P. H. Wangyang, C. H. Gong, G. F. Rao, K. Hu, X. P. Wang, C. Y. Yan, L. P. Dai, C. Y. Wu, J. Xiong, *Adv. Opt. Mater.* **2018**, *6*, 1701302.
- [7] J. Choi, J. W. Jo, F. P. G. de Arquer, Y. Zhao, B. Sun, J. Kim, M. Choi, S. Baek, A. H. Proppe, A. Seifitokaldani, D. Nam, P. Li, O. Ouellette, Y. Kim, O. Voznyy, S. Hoogland, S. O. Kelley, Z. Lu, E. H. Sargent, *Adv. Mater.* **2018**, *30*, 1801720.
- [8] B. Zhao, F. Wang, H. Y. Chen, L. X. Zheng, L. X. Su, D. X. Zhao, X. S. Fang, *Adv. Funct. Mater.* **2017**, *27*, 1700264.
- [9] T. Cossuet, J. Resende, L. Rapenne, O. Chaix-Pluchery, C. Jiménez, G. Renou, A. J. Pearson, R. L. Z. Hoyer, D. Blanc-Pelissier, N. D. Nguyen, E. Appert, D. Muñoz-Rojas, V. Consonni, Y. Deschavres, *Adv. Funct. Mater.* **2018**, *28*, 1803142.
- [10] S. Cai, X. J. Xu, W. Yang, J. X. Chen, X. S. Fang, *Adv. Mater.* **2019**, *31*, 1808138.
- [11] R. Tang, S. Han, F. Teng, K. Hu, Z. Zhang, M. Hu, X. S. Fang, *Adv. Sci.* **2018**, *5*, 1700334.
- [12] H. Choi, S. Seo, J. Lee, S. Hong, J. Song, S. Kim, S. Yim, K. Lee, S. Park, S. Lee, *J. Mater. Chem. C* **2018**, *6*, 6014.
- [13] C. de Melo, M. Jullien, Y. Battie, A. En Naciri, J. Ghanbaja, F. Montaigne, J. Pierson, F. Rigoni, N. Almqvist, A. Vomiero, S. Migot, F. Mücklich, D. Horwat, *ACS Appl. Mater. Interfaces* **2018**, *10*, 40958.
- [14] E. Zheng, X. Zhang, M. R. Esopi, C. Cai, B. Zhou, Y. Lin, Q. Yu, *ACS Appl. Mater. Interfaces* **2018**, *10*, 41552.
- [15] S. B. S. K. Sourabh Pal, *Nanoscale* **2018**, *10*, 19203.
- [16] W. Ouyang, F. Teng, M. Jiang, X. S. Fang, *Small* **2017**, *13*, 1702177.
- [17] Z. Jin, Q. Zhou, Y. Chen, P. Mao, H. Li, H. Liu, J. Wang, Y. Li, *Adv. Mater.* **2016**, *28*, 3697.
- [18] G. Li, L. Meng, X. Zhu, W. Gao, Y. Qin, L. Chen, *Nanoscale* **2018**, *10*, 2242.
- [19] J. R. D. Retamal, C. Chen, D. Lien, M. R. S. Huang, C. Lin, C. Liu, J. H. He, *ACS Photonics* **2014**, *1*, 354.
- [20] Y. Zhang, W. Jie, P. Chen, W. Liu, J. Hao, *Adv. Mater.* **2018**, *30*, 1707007.
- [21] X. Wang, P. Wang, J. Wang, W. Hu, X. Zhou, N. Guo, H. Huang, S. Sun, H. Shen, T. Lin, M. Tang, L. Liao, A. Jiang, J. Sun, X. Meng, X. Chen, W. Lu, J. Chu, *Adv. Mater.* **2015**, *27*, 6575.
- [22] D. Zheng, H. Fang, P. Wang, W. Luo, F. Gong, J. C. Ho, X. Chen, W. Lu, L. Liao, J. Wang, W. Hu, *Adv. Funct. Mater.* **2016**, *26*, 7690.
- [23] S. Joshi, S. J. Ippolito, S. Periasamy, Y. M. Sabri, M. V. Sunkara, *ACS Appl. Mater. Interfaces* **2017**, *9*, 27014.
- [24] Y. J. Kim, H. W. Park, S. D. Hyun, H. J. Kim, K. D. Kim, Y. H. Lee, T. Moon, Y. B. Lee, M. H. Park, C. S. Hwang, *Nano Lett.* **2017**, *17*, 7796.
- [25] G. Zhong, F. An, Y. Bitla, J. Wang, X. Zhong, J. Yu, W. Gao, Y. Zhang, C. Tan, Y. Ou, J. Jiang, Y. Hsieh, X. Pan, S. Xie, Y. Chu, J. Li, *ACS Nano* **2018**, *12*, 9558.
- [26] H. Lu, C.-W. Bark, D. Esque de los Ojos, J. Alcalá, C. B. Eom, G. Catalan, A. Gruverman, *Science* **2012**, *336*, 59.
- [27] N. Ma, Y. Yang, *Nano Energy* **2018**, *50*, 417.
- [28] H. Lee, T. H. Kim, J. J. Patzner, H. Lu, J. Lee, H. Zhou, W. Chang, M. K. Mahanthappa, E. Y. Tsymbal, A. Gruverman, C. B. Eom, *Nano Lett.* **2016**, *16*, 2400.
- [29] A. Gruverman, D. Wu, H. Lu, Y. Wang, H. W. Jang, C. M. Folkman, M. Y. Zhuravlev, D. Felker, M. Rzechowski, C. B. Eom, E. Y. Tsymbal, *Nano Lett.* **2009**, *9*, 3539.
- [30] R. Guo, L. Shen, H. Wang, Z. Lim, W. Lu, P. Yang, Ariando, A. Gruverman, T. Venkatesan, Y. P. Feng, J. Chen, *Adv. Mater. Interfaces* **2016**, *3*, 1600737.

- [31] J. Chen, Y. Luo, X. Ou, G. Yuan, Y. Wang, Y. Yang, J. Yin, Z. Liu, *J. Appl. Phys.* **2013**, *113*, 204105.
- [32] J. H. Zheng, Q. Jiang, J. S. Lian, *Appl. Surf. Sci.* **2011**, *257*, 5083.
- [33] J. Das, S. K. Pradhan, D. R. Sahu, D. K. Mishra, S. N. Sarangi, B. B. Nayak, S. Verma, B. K. Roul, *Physica B* **2010**, *405*, 2492.
- [34] M. Wegmann, L. Watson, A. Hendry, *J. Am. Ceram. Soc.* **2004**, *87*, 371.
- [35] J. L. Wang, J. Leroy, G. Niu, G. Saint-Girons, B. Gautier, B. Vilquin, N. Barrett, *Chem. Phys. Lett.* **2014**, *592*, 206.
- [36] C. Srilakshmi, R. Saraf, V. Prashanth, G. M. Rao, C. Shivakumara, *Inorg. Chem.* **2016**, *55*, 4795.
- [37] R. Marschall, *Adv. Funct. Mater.* **2014**, *24*, 2421.
- [38] S. Sharma, M. Tomar, N. K. Puri, V. Gupta, *Sens. Actuators, A* **2015**, *230*, 175.
- [39] S. Chala, N. Sengouga, F. Yakuphanoglu, S. Rahmane, M. Bdirina, I. Karteri, *Energy* **2018**, *164*, 871.
- [40] F. Teng, L. Zheng, K. Hu, H. Chen, Y. Li, Z. Zhang, X. S. Fang, *J. Mater. Chem. C* **2016**, *4*, 8416.
- [41] D. Buddha, *Nanoscale Adv.* **2019**, *1*, 2059.
- [42] W. Ouyang, F. Teng, J. He, X. S. Fang, *Adv. Funct. Mater.* **2019**, *29*, 1807672.